Performance and Sustainability Tradeoffs of Oxidized Carbon Nanotubes as a Cathodic Material in Lithium-Oxygen Batteries

Mark M. Falinski,*[a, b] Eva M. Albalghiti,[a, c] Andreas Backhaus,[a] and Julie B. Zimmerman*[a, d]

Climate change mitigation efforts will require a portfolio of solutions, including improvements to energy storage technologies in electric vehicles and renewable energy sources, such as the high-energy-density lithium-oxygen battery (LOB). However, if LOB technology will contribute to addressing climate change, improvements to LOB performance must not come at the cost of disproportionate increases in global warming potential (GWP) or cumulative energy demand (CED) over their lifecycle. Here, oxygen-functionalized multi-walled carbon nanotube (O-MWCNT) cathodes were produced and assessed for their initial discharge capacities and cyclability. Contrary to previous findings, the discharge capacity of O-MWCNT cathodes increased with the ratio of carbonyl/carboxyl moieties, outperforming pristine MWCNTs. However, increased oxygen concentrations decreased LOB cyclability, while high-temperature annealing increased both discharge capacity and cyclability. Improved performance resulting from MWCNT post-processing came at the cost of increased GWP and CED, which in some cases was disproportionately higher than the level of improved performance. Based on the findings presented here, there is a need to simultaneously advance research in improving LOB performance while minimizing or mitigating the environmental impacts of LOB production.

Introduction

Since the transportation sector comprises roughly 30% of global greenhouse gas (GHG) emissions, electrification of the vehicle fleet (in parallel with low-carbon electricity generation) is essential to climate change mitigation efforts.[1] However, the short range of electric vehicles relative to conventional automobiles has been a barrier to their adoption, a problem which may be remedied through the development of high-energy-density batteries[2] to replace the current lithium-ion battery (LIB) technology. Rechargeable Li–O₂ batteries (LOBs), which have a theoretical energy density roughly ten times higher than that of LIBs, have emerged as a promising replacement,[3] although significant optimization for both performance and sustainability over the life cycle is needed.

In a non-aqueous (also known as aprotic) Li–O₂ cell, lithium is oxidized in the presence of oxygen, ideally resulting in the deposition of lithium peroxide (Li_2O_2) at an oxygen-facing cathodic surface. The reverse reaction occurs during charging resulting in a high theoretic specific capacity of 3623 Wh kg^{-1} in the cell.[4–6] LOB functionality is highly reliant on close proximity between O_2 and the Li^+-containing non-aqueous electrolyte during discharge, while the reduction of O_2 occurs via the production of LiO_2 and O_2^- intermediates at or near the oxygen-facing cathode. The cathode acts a high-surface-area reaction site and also contributes to the overall battery reaction kinetics. Despite the important role of the oxygen-facing cathode, a robust understanding of how cathode properties impact LOB cell performance is lacking.

A typical LOB cathode consists of a catalyst supported by a porous current collector.[6] Carbon-based materials show great promise in this role due to their high conductivity, high surface area and pore volume, relatively low weight, and ability to cross-link with other materials through oxygen functionalizations.[7] Carbon-based LOB cathodes have been constructed using carbon nanofibers,[8,9] carbon black,[10,11] graphene,[12–14] and carbon nanotubes.[10,15,16] Of these materials, multi-walled carbon nanotubes (MWCNTs) are particularly promising and have attracted significant interest as a result;[17–19] however, previous studies have reported widely variable specific discharge capacities at the same experimental conditions for MWCNT cathodes (Figure 1),[15,16,20–26] while there are very few systematic studies to explicitly evaluate the cycling life of MWCNT cathodes as it relates to their material properties. While some of this variation may stem from differences in cathode preparation methods, binders, and electrolytes, efforts

[a] Dr. M. M. Falinski, E. M. Albalghiti, A. Backhaus, Prof. Dr. J. B. Zimmerman
     Department of Chemical and Environmental Engineering
     Yale University
     New Haven, CT 06511 (USA)
     E-mail: julie.zimmerman@yale.edu
[b] Dr. M. M. Falinski
     Department of Civil and Environmental Engineering
     Princeton University
     Princeton, NJ 08542 (USA)
     E-mail: mark.falinski@princeton.edu
[c] E. M. Albalghiti
     Department of Civil and Environmental Engineering
     University of Michigan
     Ann Arbor, MI 48109 (USA)
[d] Prof. Dr. J. B. Zimmerman
     School of the Environment
     Yale University
     New Haven, CT 06511 (USA)

ChemSusChem

Full Papers
doi.org/10.1002/cssc.202002317

Chemistry Europe
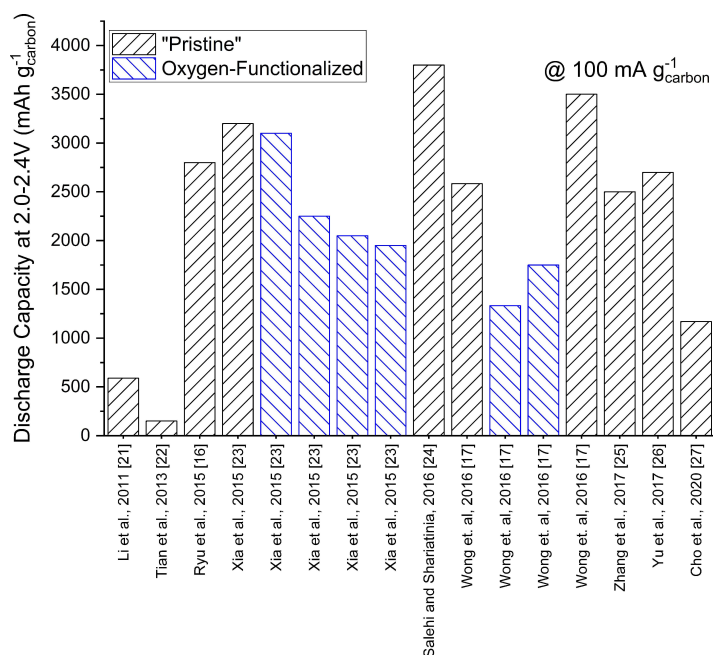European Chemical
Societies Publishing

Figure 1. Specific discharge capacity of "pristine" (black) and "oxygen-functionalized" (blue) MWCNT cathodes used in LOBs from 2011–2020 with a current density of 100 mA g$^{-1}_{carbon}$ and a final discharge potential of 2.0–2.4 V.[15,16, 20–26]

to identify the MWCNT material properties that impact performance are complicated by a lack of robust characterization.

It has been shown that MWCNT length, aggregate state, and surface can have a significant impact on both their functional performance and environmental implications.[27–29] With regard to electrochemical performance specifically, previous work has shown a relationship between surface oxygen functional group type and oxygen reduction reaction (ORR) activity or reactive oxygen species (ROS) production.[27,30] Further, the addition of oxygen functional groups, a common derivatization during or after synthesis, can yield benefits beyond electrochemical activity, as some oxygen moieties can be used as a linker to other catalysts or as reactive handles for additional functional groups.[31,32]

There have been few studies explicitly evaluating the impact of oxygen surface functionality on discharge capacity (Figure 1, blue bars) or cycling life of LOBs incorporating MWCNT cathodes. Xia et al. considered the impact of total surface oxygen content on LOB performance by oxidizing a series of MWCNTs with NaClO at varied concentrations and evaluating the specific discharge capacity and total discharge–charge cycles for each sample.[22] An increase in total surface oxygen concentration was found to yield decreased discharge capacities, while reporting no correlation between oxygen concentration and total cycling life. Still, questions remain regarding the relative impact of different oxygen functionalities, including carbonyl (C=O), carboxyl (–COOH), and hydroxy (–OH), on cycling life and discharge capacities. The use of high-temperature annealing and a wider variety of oxidizing agents offers an opportunity to assess the effects of each group.[27,33]

Wong et al. aimed to distinguish the impacts of surface oxygen groups from those of topological surface defects using oxidation and annealing techniques to produce nanomaterial with different oxygen concentration and number of defects. Oxidation was shown to lower discharge capacity, while MWCNTs that were oxidized and subsequently annealed at 900 °C had a discharge capacity between that of the oxidized samples and the untreated samples.[16] Pristine and graphitized MWCNT cathodes were able to retain capacity for 5 times as many cycles as oxidized cathodes and cathodes with defects. This may indicate that the increased oxidation and surface defects lower cycling life, contradicting the findings of Xia et al. However, since all three major functional groups are significantly reduced at the 900 °C temperature point used,[34] the potentially different impacts of oxygen surface types were not addressed.

Assessing the relationship between surface oxygen groups, concentration and/or type, and cathode performance will enable tuning of MWCNT properties according to desired design goals. However, if LOBs are to contribute to GHG emission reductions, the overall global warming potential (GWP) or cumulative energy demand (CED) resulting from realizing the target MWCNT properties should not exceed energy efficiency gains of the improved battery. The current literature on LOB cathode materials focuses primarily on improving battery capacity and achieving high cycling life, without significant consideration of the life cycle. The resulting designs have the potential to shift GHG emissions from the use phase of the car tailpipe and electrical grid to the raw material extraction or electrode production phases of the lifecycle, potentially creating a net increase in emissions.[35] For example,

ChemSusChem

Full Papers
doi.org/10.1002/cssc.202002317

Chemistry Europe
European Chemical
Societies Publishing

while MWCNTs that were graphitized at extremely high temperatures ($\approx 2800 \,^\circ$C) showed clear improvement in LOB discharge capacity and slight improvement in cycling life, this improvement was at the cost of potentially high embodied energy requirements and related GHG emissions of graphitization ovens.[36] To advance the goal of overall energy benefits from LOB technologies, evaluations of cathode materials must consider life cycle impacts alongside performance.[37] The sustainable nanomaterial selection framework[38] provides a means of selecting MWCNTs that aim to enhance performance while reducing or eliminating the negative impacts. This study aims to use this framework to assess both the performance and sustainability of several well-characterized MWCNT cathode materials with varied surface oxygen concentration and groups.

Experimental Section

Preparation of MWCNTs and inks

MWCNTs were purchased from CheapTubes (Grafton, VT, USA) and had a reported diameter of 10–20 nm and a reported length of 10–30 μm. After purchase, these were modified by a combination of oxidative processing and high-temperature annealing, some of which has been previously reported.[39] Pristine CheapTubes samples were referred to as "CT–P". Briefly, CT–P were oxidized by one of two techniques, through oxidation by refluxing nitric acid ("CT–N") or oxidation by ozonation ("CT–O"). To produce CT–N, CT was refluxed in nitric acid (HNO$_3$, 70%) for 4 h, which produced a sample with increased defects and surface oxygen functionalities. The MWCNTs were then repeatedly rinsed with deionized (DI) water and filtered to remove any residual HNO$_3$, and dried for 24 h at 100 °C. Following this, some CT–N samples underwent high-temperature annealing in an inert He atmosphere for 1 h at a maximum temperature of either 400 °C ("CT–N–400") or 600 °C ("CT–N–600"). CT–P–900 was also produced by annealing CT–P in an inert He atmosphere for one hour at 900 °C. The annealing step has the effect of reducing total surface oxygen concentration, while selectively decomposing carboxyl groups at lower annealing temperatures and decomposing hydroxy and carbonyl functionalities at higher temperatures. CT–O was produced by bubbling ozone through a room-temperature suspension of CT–P for 1 h, leading to a suspension of carbon nanotubes with an increased oxygen concentration. Ozone was generated by an Asynt Triogen LAB2B Ozone Generator. The CT–O were then rinsed with DI water and allowed to dry for 24 h at 100 °C.

The purchased and processed MWCNTs were incorporated into an ink for use in characterization and electrochemical tests. To prepare the MWCNT ink, MWCNT and binder polyvinylidene fluoride (PVDF, MTI Corporation) were added in a 4:1 ratio by mass to N-methyl-2-pyrrolidone (NMP) at a concentration of 1.5–4.5 mg MWCNT/mL NMP and allowed to bath sonicate for 1 h at room temperature, yielding a well-dispersed slurry.

Material characterization

The structures, properties, and composition of the MWCNT samples used in this study were characterized by X-ray photoelectron spectroscopy (XPS), scanning electron microscopy (SEM), transmission electron microscopy (TEM), Raman spectroscopy, Brunauer–Emmett–Teller (BET) surface area measurements, modified two-probe conductivity measurements, and X-ray diffraction

analysis (XRD). Elemental analysis by XPS was performed using a Physical Electronics PHI VersaProbe II Scanning XPS Microscope (Chanhassen, MN, USA). XPS was able to provide the relative atomic percentage of carbon and oxygen for a given MWCNT sample. The carbon and oxygen peaks provided by XPS could also be deconvoluted to approximate the relative abundance of oxygen moieties on the surface, specifically carboxyl, hydroxyl, and carbonyl functional groups. Further, to more accurately quantify the relative atomic percentage of each oxygen moiety, a chemical derivatization technique, coupled with XPS (CD-XPS), was also utilized, as explained in other work.[33] Briefly, the fluorinated molecules trifluoroacetic anhydride, trifluoroethylhydrazine, and trifluoroethanol (with di-tert-butyl carbodiimide) selectively react with hydroxy, carbonyl, and carboxyl functionalities, respectively. Then, using XPS, the atomic ratio of fluorine to carbon can be determined and back-calculated to determine the amount of each oxygen functional group relative to the total surface oxygen content. It is worth noting that due to the nature of the chemical derivatization reactions, results become less accurate at lower oxygen group concentrations. Therefore, CD-XPS was only employed to study the oxidized MWNCT samples (CT–N, CT–N–400, CT–N–600, CT–O). SEM imaging was done using a Hitachi SU-70 scanning electron microscope. SEM was used to confirm MWCNT sample maintained its tube-like structure after undergoing harsh oxidative techniques. In order to improve MWCNT image quality on SEM, a thin Ir layer ($\approx$1–3 nm) was coated on the surface. SEM, in conjunction with image analysis using ImageJ (NIH), was used to determine length distributions of pristine and nitric acid-treated MWCNTs to ensure relatively similar length distributions. Raman spectroscopy was performed on the MWCNT ink to ensure a high signal and was done by using a LabRAM HR Evolution system. BET specific surface area measurements were done on MWCNT powders using a Micromeritics ASAP 2460, at an analysis bath temperature of 77.3 K. Conductivity measurements were done using a BioLogic VMP3 electrochemical workstation via a two-probe conductivity measurement of MWCNT ink that was drop cast onto a cleaned glass slide and allowed to dry into a film.

Electrochemical characterization

The cathodes for Li–O$_2$ batteries was produced by dropping 20–60 μL of MWCNT ink on Ni foam (MTI Corporation, CA, USA) and allowing it to dry overnight under vacuum at 90 °C. After NMP was evaporated, the cathode was weighed and transferred to an Ar-filled glovebox. Each 2032 coin cell was assembled in a dry Ar glovebox with <0.5 ppm H$_2$O and <3 ppm O$_2$, with an Li foil anode, two Whatman glass separators covered in the electrolyte [1 M lithium bis(trifluoromethanesulfonyl)imide (LiTFSI) in tetraethylene glycol dimethyl ether (TEGDME)], and the oxygen-facing cathode at the top of the coin cell, where there is a large hole open to the surrounding environment. The crimped coin cell was placed into a large glass chamber, which was then purged with a steady flow of ultra-high-purity oxygen to removed Ar and fill the chamber with O$_2$. The chamber was then allowed to rest for at least 4 h to allow for cell stabilization. All battery performance was evaluated over the voltage range of 2.0–4.5 V vs. Li/Li$^+$ using a BioLogic VMP3 electrochemical workstation.

For initial discharge measurements, the LOBs were discharged at a rate of 100 mA g$^{-1}_{carbon}$ until the potential reached a value of 2.0 V. Cyclability of each LOB system was determined by discharging then charging LOBs at a rate of 500 mA g$^{-1}_{carbon}$ either to a capacity of 1000 mA h g$^{-1}_{carbon}$ or to a discharge potential of 2.0 V or a charging potential of 4.5 V.

ChemSusChem

Full Papers
doi.org/10.1002/cssc.202002317

**Chemistry
Europe**
European Chemical
Societies Publishing

Life Cycle Assessment methodology

Goal and scope: The goal of this work was to examine the GHG emissions and CED of both the synthesis and post-synthesis processing (PSP), such as oxidation and annealing, of MWCNTs at the lab-scale for LOBs. In doing so, we can better understand the relative impacts of PSP.

Functional unit: The functional unit in this study is 1 g of MWCNT material. In this, we assume that the oxidation or annealing of MWCNTs does not significantly alter the mass, and that the mass input and output for each PSP step stays constant.

System boundary: This study considers a cradle-to-gate boundary system, which is cut off at the end of MWCNT production. Since Teah et al.[40] did not quantify the emissions to the environment as a result of unreacted precursors and byproducts, emissions to the environment were not considered for any of the processing or PSP steps, including those explicitly stated by Trompeta et al.,[41] in an effort to remain consistent. Model inputs/outputs can be found in the Supporting Information.

LCI and LCIA: The life cycle inventory (LCI) database we used for material acquisition and electricity generation was from Ecoinvent v3.6, a commonly used LCI database. For electricity generation, we used the dataset that was specific to the US electricity mix, and for other materials, we defaulted to markets for materials in either the rest of world or the global market. For materials not in the database (specifically ferrocene and aluminum isopropoxide), stoichiometric relationships were employed to model the chemicals, as previously described.[38] The LCIA model was created in OpenLCA v1.10.2, and the IPCC impact assessment method was used to determine the 20-year global warming potential of the MWCNT synthesis and PSP, while the cumulative energy demand method was used to calculate CED.

Error calculations: Since this study focuses on the impact of post-synthesis processing on LOB performance, the CED and GWP of each sample's processing was determined by Monte Carlo simulation (500 iterations). Based on the results of that analysis, both average values and error could be determined.

Other assumptions: There is a lack of studies explicitly looking at the relationship between reaction conditions and MWCNT length during fluidized bed chemical vapor deposition (FB-CVD). As a result, it is difficult to approximate how reaction conditions would change for the FB-CVD case used in this study to produce shorter MWCNTs that are more similar in length to those provided by CheapTubes (10–30 μm in length). It is possible that the production of the same functional unit of the shorter CheapTubes would actually require a higher GWP, since either a higher number of reactions or more catalysts would be required to produce the same mass. Therefore, the values provided by Teah et al. were used to model MWCNT growth, but it is of note that this is likely a low estimate.

The reported length of MWCNTs produced by the work of Trompeta et al. (>10 μm) was more similar to those purchased from CheapTubes. The CNT synthesis modeled in that work was also far more optimized than the work of Teah et al. or the PSP done in our lab. This makes the relative GWP and CED of PSP seem much higher, and it is therefore safe to assume that if PSP was also optimized to the same extent, that step would have lowered energy use and emissions. This is also noted in the main document.

Finally, since the catalysts used by Trompeta et al. were not regenerated for reuse, the model system chosen from Teah et al. was their system, labeled CVD_Ar_1, where catalysts were also used once without regeneration.

Results and Discussion

MWCNT characterization

MWCNTs were oxidized by various oxidants and annealed at different temperatures after purchase. The manufacturer confirmed that the purchased MWCNTs were produced using CVD. Following post-synthesis processing, XPS and Raman spectroscopy were used to assess total surface oxygen concentration and I_D/I_G ratio, respectively, and those as well as sample names, post-processing procedures, and the chemical and physical properties of each sample can be found in Table 1, along with the specific surface area and conductivity of each sample.

Nitric acid was used to oxidize several MWCNT samples. Since acidic oxidants have been shown to cut carbon nanotubes in a treatment time-dependent manner,[42] a treatment time of 4 h was chosen to limit cutting and retain consistent lengths between samples, while still imparting surface functionalities.[43] Measuring MWCNT length is a particularly difficult task, especially for samples with a higher reported length, due to sample tangling. However, SEM image processing of 100–200 MWCNTs per sample did show an overlapping length distribution for untangled CT–P and CT–N nanotubes, confirming the assumption that length distributions remain relatively similar after oxidation (Figure S1). Neither ozone-based oxidation techniques[44] nor high-temperature annealing under inert gas[45] have been shown to affect length significantly. Therefore, the samples are assumed to be of roughly equal length.

Table 1. MWCNT sample names, treatment steps, oxygen concentration, I_D/I_G ratio as determined by Raman spectroscopy, specific surface area, and conductivity.[a]

Sample	Treatment	Oxygen concentration [%]	I_D/I_G	Specific surface area [m² g⁻¹]	Conductivity [mS m⁻¹]
CT–P	untreated	1.0	1.16 ± 0.02	135.7	254.1 ± 118.7
CT–P–900	annealed under He at 900 °C	0.5	1.18 ± 0.01	140.3	60.6 ± 19.4
CT–N	refluxed in HNO₃ for 4 h	7.0	1.56 ± 0.04	221.3	43.0 ± 9.8
CT–N–400	refluxed in HNO₃ for 4 h, annealed under He at 400 °C	3.5	1.61 ± 0.05	234.6	33.2 ± 9.5
CT–N–600	refluxed in HNO₃ for 4 h, annealed under He at 600 °C	2.8	1.62 ± 0.13	217.1	4.4 ± 1.8
CT–O	oxidized by ozonation in water for 1 h	4.0	1.36 ± 0.02	180.2	65 ± 11.3

[a] For all samples: reported diameter: 10–20 nm; reported length: 10–30 μm; manufacturer: CheapTubes.

ChemSusChem

Full Papers
doi.org/10.1002/cssc.202002317

Chemistry Europe
European Chemical
Societies Publishing

Surface oxygen concentration

In accordance with well-established trends,[33,39] the total oxygen concentration increased when pristine MWCNTs were treated with nitric acid and ozone, while high-temperature annealing of CT–N and CT–P samples decreased overall oxygen concentration, with greater decreases occurring at higher temperatures. As a measure of surface defect concentration, the I_D/I_G ratio was determined using Raman spectroscopy (for sample spectra, see the Supporting Information, Figure S2). As samples were oxidized by nitric acid and ozonation, the I_D/I_G ratio increased with increasing oxygen percentage (Figure S3). This is due to oxygen functionalities contributing to the creation of surface defects at the nanotube edge and basal plane, decreasing the overall graphitic nature of the carbon nanotubes and thereby increasing the presence of the D-band.[46] Ozonation increases I_D/I_G ratio to a lesser extent than acid treatment, since ozonation leads to less damage to the sp^2 lattice.[47] As the oxygen functionalities are reduced via high-temperature annealing, the I_D/I_G ratio does statistically significantly change. This indicates a reduction of surface oxygen without significant defect healing, due to the formation of topological defects at sites where oxygen functionalities were located.[48] While the temperatures used in this study can selectively reduce carboxyl functionalizations,[27] leaving behind a hole in the basal plane due to the removal of carbon atoms during the initial carboxylate defect formation,[49] complete healing of MWCNT surface defects requires annealing temperatures far above those used in this study.[34]

Total surface oxygen concentration is not the best predictor of electrochemical activity, and as a result, the relative concentration of specific oxygen moieties must also be quantified for each MWCNT sample. This was achieved through two complementary strategies. First, the C 1 s peak from XPS was deconvoluted to reveal peaks at 284.8 eV (C–C, C=C), 285.5 eV (C–OH), 286.7 eV (C=O, C–O–C), 289.4 eV (–COOH), and 292 eV (π-π^*). Each peak was integrated, revealing the relative quantity of each of the three moieties of interest: carboxyl (–COOH) groups, hydroxy groups (–OH), and carbonyl groups (C=O).[22]

Due to the occasionally subjective nature of peak deconvolution,[33] functional group ratios were also confirmed using CD-XPS. Briefly, select MWCNTs were derivatized by 2,2,2-trifluoroethanol with di-*tert*-butylcarbodiimide and pyridine, trifluoroacetic anhydride, and 2,2,2-trifluoroethylhydrazine to quantify the ratios of –COOH, –OH, and C=O, respectively, to total oxygen concentration as detailed previously by Wepasnick et al. and in further detail in the Supporting Information.[33] The deconvoluted XPS spectra and ratios of oxygen moieties to total oxygen are show in Figure 2.

Since nitric acid oxidation primarily results in carboxylation,[33] an expected decrease in the ratio of carbonyl/carboxyl moieties upon oxidation by nitric acid is observed. However, as previously reported,[33] the ratio of carbonyl/carboxyl moieties is significantly higher when the pristine MWCNTs are oxidized by ozone rather than nitric acid. Further, as annealing temperature increases, the carbonyl/carboxyl
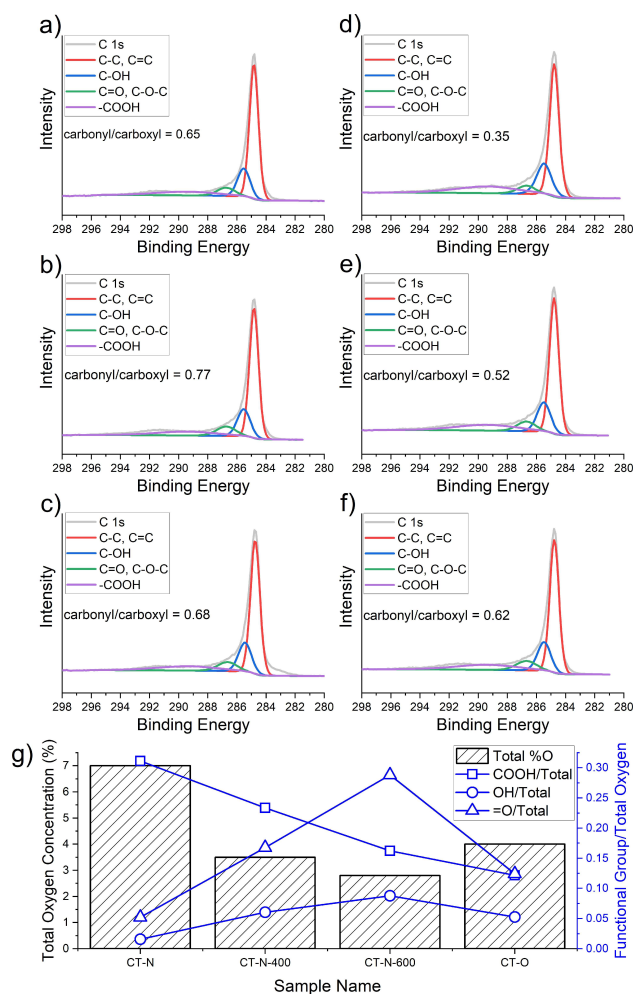

Figure 2. Deconvoluted XPS C 1 s spectra for (a) CT–P, (b) CT–P–900, (c) CT–O, (d) CT–N, (e) CT–N–400, and (f) CT–N–600. (g) Total oxygen concentration with ratios of each functional group to the total percent oxygen as determined by CD-XPS.

moiety ratio increases, likely due to a reduction of carboxyl groups at basal and edge sites with increasing temperatures. Notably, carbonyl functionalities generally begin to degrade at temperatures of 900 °C or higher.[50] CD-XPS results agreed with results from deconvoluted peak analysis, showing the same trend for the carbonyl/carboxyl moiety ratio (e.g., an increase in the ratio of carbonyl groups to carboxyl groups due to carboxyl reduction). It is worth noting that, while CD-XPS can be a powerful technique with high levels of accuracy at appropriately high surface oxygen concentrations, accuracy may be reduced at lower oxygen concentrations (less than 3%). For this reason, CD-XPS was not used to evaluate CT–P or CT–P–900, but the results from CD-XPS analysis for the other four samples were generally considered to be more reliable than the deconvoluted C 1s peak. As a result, when considering the concentration of various oxygen moieties, the results from CD-XPS were the default.

ChemSusChem

Full Papers
doi.org/10.1002/cssc.202002317

Chemistry Europe
European Chemical
Societies Publishing

Lithium–oxygen battery performance

The performance of each MWCNT sample as the oxygen-facing cathode in a Li–O$_2$ cell was assessed by measuring cell discharge capacity and cycling performance. Briefly, coin cells were constructed containing a lithium foil anode, a MWCNT nanoink and nickel foam cathode, two glass filter separators, and an electrolyte composed of 1 M LiTFSI in TEGDME. Cells were assembled in a dry argon glovebox and placed in glass

containment units, which were purged with oxygen and allowed to equilibrate. Total discharge capacity was determined by discharging the equilibrated cell at a current of 100 mA g$^{-1}_{carbon}$ until it reached a potential of 2.0 V (Figure 3a). The normalized capacity at 2.0 V was the discharge capacity.

Previous studies have found that an increase in oxygen concentration correlates strongly with a decrease in total discharge capacity.[16,22] However, each study only used one type of oxidant (either NaClO or H$_2$SO$_4$/HNO$_3$) at either varying
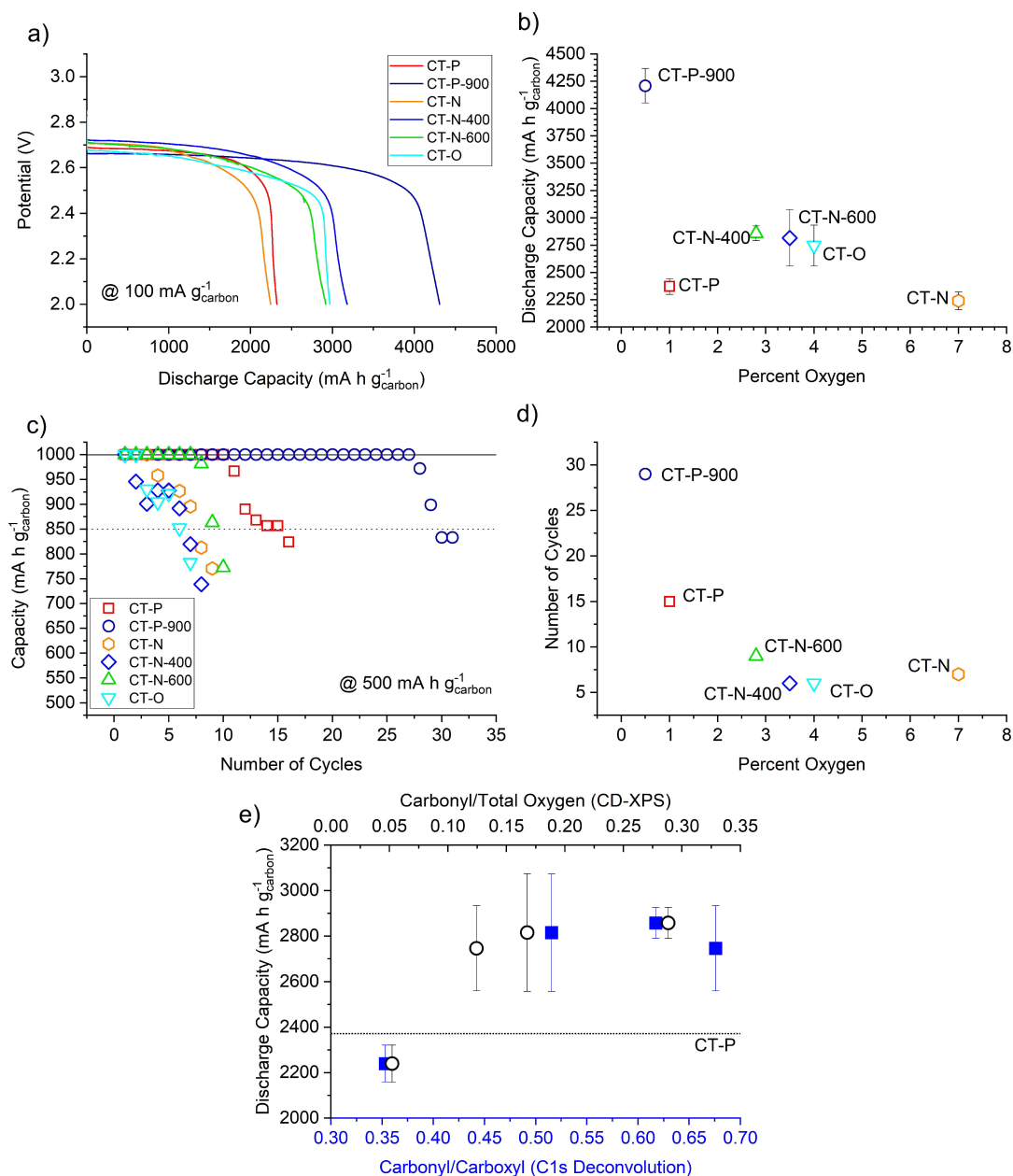

Figure 3. Discharge capacity and cycling performance of oxidized MWCNTs. (a) Representative data for the potential as a function of capacity in single-cycle runs for one discharge cycle at a rate of 100 mA g$^{-1}_{carbon}$. (b) Maximum discharge capacity of each sample as it relates to total surface oxygen concentration, measured in triplicate (errors bars represent the standard deviation of measurements). (c) Capacity for each cell at a discharge and charge rate of 500 mA g$^{-1}_{carbon}$ at a maximum capacity of 1000 mAh g$^{-1}_{carbon}$ as determined through single experiments. (d) Cycle number at which the capacity reached during cycling experiments dropped below 850 mAh g$^{-1}_{carbon}$ as related to surface oxygen concentration [%]. (e) Capacity for each of the oxidized MWCNT samples related to the carbonyl/carboxyl ratio and the carbonyl/total carbon ratio, where the horizontal dotted line indicates the discharge capacity of the untreated MWCNT sample (CT–P).

ChemSusChem

Full Papers
doi.org/10.1002/cssc.202002317

Chemistry
Europe
European Chemical
Societies Publishing

times or concentrations, which led to relatively consistent ratios of each of the three common oxygen moieties. Specifically, for MWCNTs functionalized by NaClO, there was a greater relative abundance of hydroxy and carboxyl groups, which increased as oxidation time increased,[22] while for those functionalized by H_2SO_4/HNO_3, the primary oxygen moiety was carboxyl groups, as noted elsewhere in the literature.[33]

As indicated by the results reported by those studies, the most carboxylated MWCNT sample (CT–N) was found to have a reduced discharge capacity relative to its pristine counterpart (CT–P) (Figure 3b). However, an increase in total oxygen concentration did not always correlate with a decrease in discharge capacity; three samples (CT–N–400, CT–N–600, and CT–O) had a higher surface oxygen concentration than their pristine counterpart, but still had an increased average discharge capacity (Figure 3b). Surface oxidation can also impact MWCNT specific surface area and conductivity, which in turn has been linked to discharge capacity and cyclability. However, there appears to be no relationship between surface area or conductivity and the performance of the battery systems in this study (Figure S4). This suggests that increased oxygen concentration and the related physicochemical differences of MWCNT samples does not always result in a decreased capacity, and instead, the different oxygen moieties can play a role in total discharge capacity.

The MWCNT property which best predicts initial discharge capacity is the carbonyl/carboxyl ratio, as shown in Figure 3e. Specifically, a carbonyl/carboxyl ratio higher than 0.50, as determined by deconvolution of C1s peaks, (i.e., higher relative amount of carbonyl functionalization) was related to a higher capacity. Also, based on CD-XPS, oxidized MWCNTs where carbonyl functionalities composed more than 10% of oxygen moieties were also related to higher discharge capacity. These results suggest that the elimination of carboxyl functionalities via annealing, or minimizing them by using ozone for oxidation, may help to improve discharge capacity. This is likely due to two competing impacts: 1) the enhanced sorption of O_2 molecules and the enhanced redox nature of carbonyl-containing groups, and 2) the preventative effects of surface carboxylation.

There are multiple studies linking carbonyl-type groups to an increase in electrochemical activity.[27,51–53] Carbonyl groups in MWCNTs have been shown to have a higher work function (e.g., the minimum energy necessary to free the electron from the surface) than both carboxyl functionalizations and defect sites.[54] Since the discharging and charging of Li–O_2 batteries depends on oxygen reduction reaction (ORR) activity, the increase in work function by carbonyl groups is likely linked to better discharge performance.

Another reason that increased carbonyl groups relative to carboxyl groups may result in increased capacity is due to the role of steric hindrance and oxygen sorption. Due to the immeasurably short lifetime and diffusion coefficient less than $2 \times 10^{-6}\,\mathrm{cm^2\,s^{-1}}$ in common aprotic solvents of reactive oxygen species and their role in ORR, the reactants (in this case, lithium ions and oxygen) must be incredibly close to the site at which electron transfer occurs.[55,56] As a result, electron transfer

requires oxygen molecules to interact directly with the carbon surface through physisorption or chemisorption. Density functional theory (DFT) models have shown that the energy required for adsorption of oxygen molecules to graphitic surfaces near carboxyl moieties is nearly twice that of the same process near carbonyl moieties.[57] This indicates that the presence of carboxyl functionalities makes the physisorption of oxygen molecules less likely, while the physisorptive interactions of oxygen molecules with graphitic surfaces containing carbonyl are more stable.[57] Other DFT models have found that the carboxyl group itself interacts only weakly with O_2 molecules, while the interaction between pristine and defective CNT surfaces can lead to physisorption and chemisorption, respectively.[58] It has been reported that the presence of many surface groups may prevent catalytic activity via steric hindrance, and the polar carboxyl groups can form hydrogen bonds preventing access to the basal plane or the more electrochemically active carbonyl functionalities.[50]

While select oxygen moieties contribute to improved discharge capacities, changes in oxygen functional group type do not drastically improve the total cyclability of the LOBs, and instead, cycling capacity decreases with increased oxygen concentration (Figure 3c–e). The annealed sample (CT–P–900) cycled almost twice as many times as CT–P, but CT–N, CT–N–400, CT–N–600, and CT–O have worse cycling performance than the pristine cathode. This suggests that there are other factors contributing to cyclability beyond electrochemical activity during discharge and charge, such as the production of lithium-based species that can block reactive sites.

In an idealized discharge process, oxidized lithium products, particularly Li_2O_2, form on the surface of the air facing cathode. Those products are then reduced back to Li^+ and O_2 during charge and reactive sites are then re-exposed to allow for further reactions during the next discharge cycle. However, it is likely that this ideal reaction is not the only reaction occurring, limiting the cyclability of all oxidized samples. For example, carboxyl groups and defects can contribute to the production of parasitic Li_2CO_3 at the cathode surface, thus blocking of reactive sites by oxidized lithium products.

More disordered carbon, especially that which contains carboxyl groups, aids in the production of parasitic Li_2CO_3 at the cathode surface and contributes to the blocking of reactive sites over time.[53] DFT modeling has shown graphitic materials with more defects are more likely to participate in chemisorption than pristine, undamaged surfaces.[58–60] Once O_2 is chemisorbed, it can lead to the stabilization of Li-oxygen species, which can further stabilize LiO_2 in an adsorbed form, leading to an adsorbed form of Li_2O_2 or Li_2CO_3, blocking electrochemically reactive sites.[59,61] It has also been shown that functional groups, especially carboxyl groups and structural defects that stabilize Li_2O_2, lead to the degradation of electrolytes and can further the formation of parasitic Li_2CO_3, which can cyclically reduce the stability of the cell.[53,62] Meanwhile, samples with very low defect site density (such as CT–P–900) tend to have far less lithium on the surface after recharging than after discharging, likely due to a lack of chemisorptive sites.

ChemSusChem

Full Papers
doi.org/10.1002/cssc.202002317

Chemistry Europe
European Chemical
Societies Publishing

As discussed previously, defects generally begin healing at temperatures exceeding those used in this study.[34,50] The similar I_D/I_G ratio for CT–N, CT–N–400, and CT–N–600, even with varied oxygen content, indicate that the defects are not healing as a result of the additional annealing. These defects sites that are left behind by decarboxylation can become chemisorptive sites, stabilizing oxidized lithium, leading to physically blocked reactive sites. CT–N likely perform so poorly due to its already low number of electrochemically active sites and the abundance of carboxylation that can aid in the production of Li_2CO_3. Further, while CT–P is relatively pristine compared to most of the other samples based on Raman spectroscopy, its lack of cyclability is also likely a result of the formation of Li_2CO_3. This may be due to the presence of amorphous carbon left over during production that was not removed via oxidative treatment or annealing.[59,63]

More sustainable MWCNT Li–O$_2$ batteries

While it has been demonstrated that improved performance of LOBs can be achieved by adjusting MWCNT surface chemistry, these improvements must not come at the cost of eradicating the energy efficiency gains. To evaluate the potentially energy consumption and negative environmental impacts of post-synthetic processing of MWCNTs, a lab-scale life cycle assessment (LCA) was conducted to determine the cradle-to-gate GWP in kilograms of CO_2-eq released per gram of MWCNT sample produced, based on the IPCC 2013 Life Cycle Impact Assessment (LCIA).[64] Additionally, an assessment of CED was done using the cumulative energy demand LCIA.[65] All calculations were done in OpenLCA v1.10.2, and Monte Carlo simulations were used to determine the GWP or CED calculation error as a result of post-synthesis processing. Results from these impact assessments were then combined with data on performance (measured as discharge capacity and cycling life) to create two-dimensional charts, as outlined by the sustainable nano-material selection framework.[38]

The manufacturer, CheapTubes, reported CVD as the preferred method of MWCNT synthesis, so the LCAs used in this assessment assumed production via CVD. Of note, due to the relative unknowns regarding scaling of MWCNT production processes, and the proprietary nature of commercial data, lab-scale processes are used based on the work of Teah et al.,[40] who modeled the lab-scale production of long, pure MWCNT (> 300 μm) in a fluidized bed CVD (FB-CVD) system, and Trompeta et al.,[41] who modeled a more optimized lab-scale production of shorter (> 10 um) MWCNT in a hot-wall CVD reactor (HW-CVD). In both studies, energy and material inputs during synthesis were collected at the lab-scale using flow-meters and other indicators. A similar strategy to model material and energy inputs during post-synthesis processing in our lab was followed. Further details regarding data collection, assumptions, and model inputs can be found in the Supporting Information. Of note, due to the nature of lab-scale production methods, it is likely that scaling up and optimizing a full-scale process and post-synthesis processing would decrease the GWP and/or CED

for each MWCNT sample.[66] This is likely even more applicable for the FB-CVD analysis, since it is not nearly as optimized as the production of MWCNTs using the HW-CVD system by Trompeta et al.[41] However, until data about the industrial production and post-synthesis processing of MWCNTs are more readily available and reliable, lab-scale data will be used.

As expected, the lab-scale GWP and CED of all annealed and oxidized samples were higher than the initial, pristine sample, CT–P, as produced by FB-CVD or HW-CVD (Figure 4). However, the variability in the magnitude of GWP and CED should be noted. When considering the lab-scale production requirements for a FB-CVD system, CT–O yielded an increase in GWP and CED of about 1–2% over that of CT–P, while acid treated and annealed samples saw an increase in GWP and CED of more than 10 and 17%, respectively. This is due to the energy demands of high-temperature annealing, and the embedded GHG emissions related to refluxing nitric acid as well as the relative to the demands of ozone production.

However, just considering the total GWP and CED increase cannot be used to select the most sustainable *and* highest performing material, and as such, both GWP/CED and discharge capacity must be considered in tandem, through the use of impact/benefit ratios.[28] One way to do this is relative to a defined base case. The blue and black line on Figure 4a represents the ratio of GWP/performance and ratio of CED/performance, respectively, of the base case (CT–P via FB-CVD). Any points along those lines have the same ratios of impact/benefits as CT–P (the base case). Samples to the left of those lines, such as CT–N, produce more GHGs or require more energy per unit of capacity or cycling, indicating that they are not beneficial to pursue from the perspective of energy efficiency gains, due to a worse ratio of impacts to benefits than the base case. Meanwhile, samples to the right of the lines are good candidates for further exploration, due to their relatively low GHG emissions or energy requirements relative to increases in performance. In fact, when the pristine MWCNT sample is produced by FB-CVD, post-synthesis processing appears to be worth the tradeoff of a higher GWP and CED to achieve a higher discharge capacity. Further, of the four post-synthesis processes, the most promising technique to pursue as indicated by this analysis would likely be annealing at 900 °C (CT–P–900), since it has the lowest impact/benefit ratio of GWP and CED to discharge capacity (Table 2).

When cyclability is instead used as a measure of performance, the life cycle functional unit can be defined as one discharge–charge cycle at a rate of 500 mA g^{-1}$_{carbon}$ to a maximum capacity of 1000 mA h g^{-1}$_{carbon}$. The only sample that shows a significant decrease in relative CED and GWP per cycle is CT–P–900, which requires roughly half of the energy during production of the pristine MWCNT, and produces roughly half of the GHG emissions of CT–P. This indicates that the CT–P–900 cathodes perform at a high enough level to overcome the added negative implications related to post-synthesis processing (Figure 4c, Table 2).

When the synthetic method used to produce the pristine MWCNT is instead the more optimized HW-CVD method, the impacts of post-synthesis processing appear to be relatively
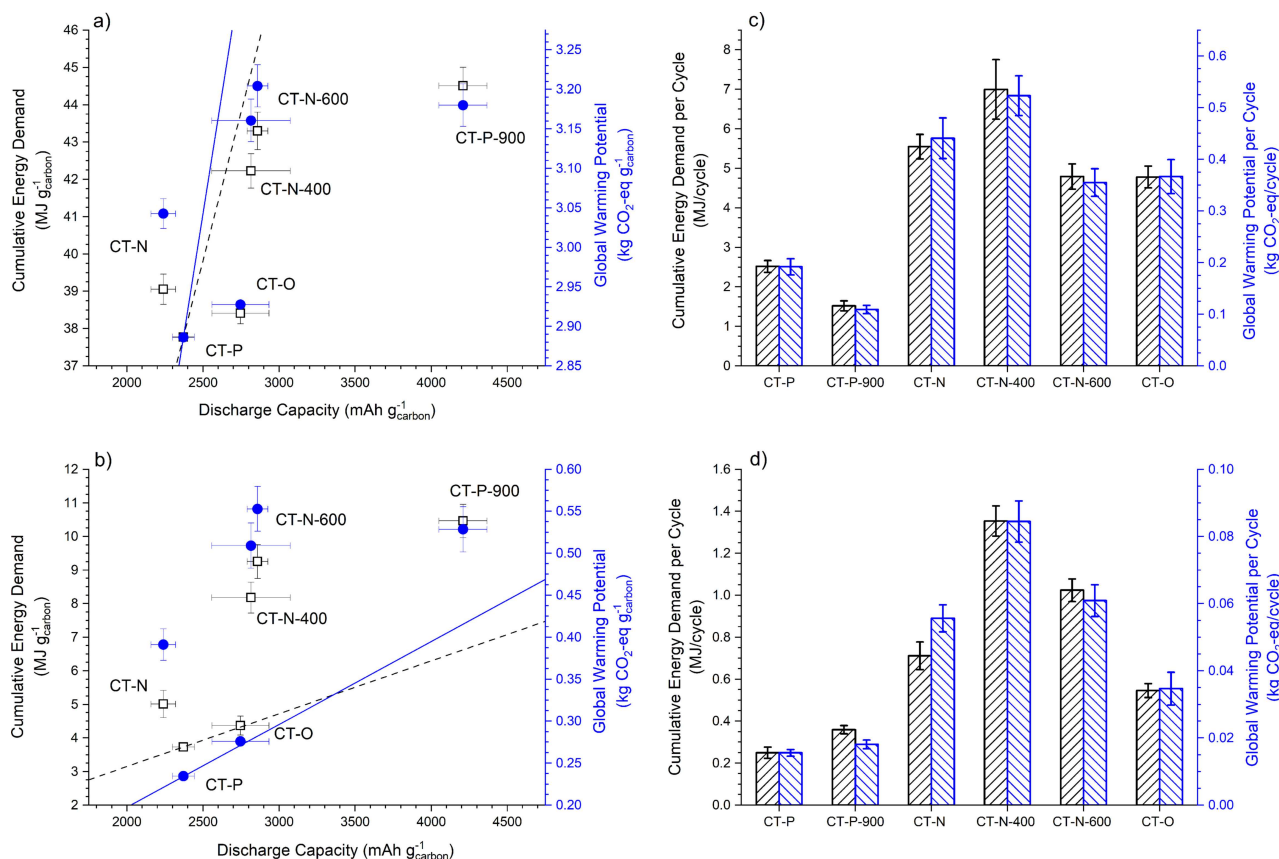
ChemSusChem

Full Papers
doi.org/10.1002/cssc.202002317

Chemistry
Europe
European Chemical
Societies Publishing

Figure 4. Two-dimensional Ashby-like charts showing the GWP of producing and functionalizing MWCNTs at the lab scale versus discharge capacity where the initial MWCNT is produced via (a) FB-CVD[40] and (b) optimized HW-CVD.[41] CED and GWP per functional unit (1 cycle) for MWCNT produced via (c) FB-CVD[40] and d) optimized HW-CVD,[41] where all y-error bars are determined by Monte Carlo analysis.

Table 2. Impact/benefit ratios for each MWCNT cathode sample, where impact is defined as either GWP [kg CO_2-eq] or CED [MJ] and benefit is defined as either capacity [mA h g^{-1}_{carbon}] or total cycling life.

Method	Impact/benefit	Sample CT–P	CT–P–900	CT–N	CT–N–400	CT–N–600	CT–O
FB-CVD	GWP/capacity	1.20E-03	7.56E-04	1.33E-03	1.09E-03	1.10E-03	1.07E-03
	CED/capacity	1.58E-02	1.06E-02	1.70E-02	1.46E-02	1.49E-02	1.40E-02
	GWP/cycles	1.92E-01	1.09E-01	4.41E-01	5.23E-01	3.55E-01	3.66E-01
	CED/cycles	2.52	1.52	5.55	7.00	4.79	4.78
HW-CVD	GWP/capacity	9.78E-05	1.26E-04	1.71E-04	1.76E-04	1.90E-04	1.01E-04
	CED/capacity	1.56E-03	2.49E-03	2.19E-03	2.83E-03	3.18E-03	1.59E-03
	GWP/cycles	1.55E-02	1.81E-02	5.56E-02	8.44E-02	6.09E-02	3.47E-02
	CED/cycles	2.49E-01	3.59E-01	7.10E-01	1.35E+00	1.02E+00	5.45E-01

higher. This is in part due to the varied levels of optimization or production (i.e., the MWCNT synthesis step is optimized for reduced environmental impact, while post-synthesis processing is not fully optimized), and in part due to general improvements in MWCNT syntheses processes over time. This offers an interesting case study for continued improvement in MWCNT syntheses. As synthesis becomes more sustainable, it becomes more difficult to justify post-synthesis processing as a means to improve performance of LOBs. For example, while 4 of the 5 processed MWCNTs had higher CED/discharge and GWP/discharge ratios than the base case for the FB-CVD scenario, only one (CT–O) has similar ratios to the base case when

MWCNTs are synthesized by HW-CVD (Figure 4b). This indicates that, under a circumstance where MWCNT synthesis is more optimized, the more environmentally friendly approach to increase total discharge capacity would be to use a higher mass of pristine MWCNTs in the cathode, rather than using a similar mass of an oxidized or annealed set of MWCNTs, since total discharge capacity increases with increasing cathode mass.[67]

When performance is instead defined by the cyclability of each cathode and the initial MWCNT synthesis is more optimized, the pristine MWCNT has the lowest CED and GWP per completed cycle. There are no post-processing techniques from this study that show a high enough improvement in

ChemSusChem

Full Papers
doi.org/10.1002/cssc.202002317

Chemistry Europe
European Chemical
Societies Publishing

cyclability to outweigh the environmental impacts of the post-processing of optimally produced MWCNT cathodes (Figure 4d). Instead, increasing mass of CT–P in the cathode is a more environmentally friendly way to increase cyclability. As mass increases, the normalized discharge rate and capacity would decrease, which would increase the total number of cycles an LOB could experience before failure.[68]

Of note, the results and conclusions related to CED and GWP are specific to this system, which does not contain any metallic or metal oxide catalysts in the cathode to enhance electrochemical reactions, and thus LOB cyclability.[15] However, the lessons gleaned here should also be applied to future LOB cycling experiments. The addition of rare metals and structure changes to nanomaterials used on the cathodic side of LOBs can act to improve discharge capacity and/or cyclability of emerging LOB systems, but it will continue to be imperative to ensure that the energy and GHG emissions resulting from these improvements do not outweigh the benefits of the technology felt at the use phase. Therefore, as synthetic methods for MWCNTs and other potential cathodic materials continue to improve and become more sustainable, an effort must be put into 1) decreasing the environmental and energy impacts of processing that results in a higher performing LOB and 2) further improving performance of LOBs by optimizing structure-property-function relationships of materials, including MWCNTs, found in cathodes.

Conclusions

Improved use of multi-walled carbon nanotubes (MWCNT) and other carbonaceous materials in lithium–oxygen battery (LOB) systems will require a more thorough understanding of the impacts of physicochemical properties on battery performance, as well as the negative impacts related to the synthesis and functionalization of MWCNTs. While other researchers have found that the addition of oxygen surface moieties decrease discharge capacity, we report that under the right circumstances, the addition of oxygen moieties can actually lead to an increase in capacity. Specifically, the opposing roles of carboxyl and carbonyl functional groups was the best predictors of initial discharge capacity, where an increased capacity correlated with an increase in carbonyl moieties and a decrease in carboxyl moieties. However, this increased discharge capacity does not necessarily translate to increased cyclability, as defects and the sorptive properties of difference functional groups and of pristine MWCNT walls can also be linked to Li build-up on cathode surfaces.

Unsurprisingly, post-synthesis processing increased global warming potential (GWP) and cumulative energy demand (CED) for every sample, but many of the higher-performing MWCNT samples also had a higher impact/benefit ratio (e.g., GWP/discharge or CED/discharge) than the pristine MWCNT, meaning the life cycle impacts may not necessarily outweigh the gains in discharge capacity. However, only highly annealed MWCNTs also had an improved impact/benefit ratio when the benefit

was defined as cycling life, indicating that the most promising post-synthesis processing step is just annealing.

LOBs show a lot of promise for the future of electric vehicles and other energy storage applications. However, the design of the electrodes used in these technologies must be focused on both improving the capacity and cyclability and decreasing the negative impacts related to their use. Therefore, future research in this space should aim to address two questions. First, if carbonaceous nanomaterial-based cathodes (CNTs, graphenes, fullerenes, cellulose, nano-carbon black, etc.) are to be used in future LOB technologies, how can physicochemical structures and properties such as surface chemistry and size be optimized to be improve performance? Second, how can environmental impacts, including those that impact eco- and human health, be minimized or eliminated during production of nanomaterials and other electrodes used in LOBs? These questions will require collaboration between material scientists, toxicologists, electrical engineers, and environmental scientists, but answering them will enhance the likelihood of safer and more sustainable development of LOB technologies, and subsequently, climate change solutions.

Conflict of Interest

The authors declare no conflict of interest.

[1] R. Á. Fernández, *J. Cleaner Prod.* **2019**, *218*, 476–485.
[2] L. Noel, G. Zarazua de Rubens, B. K. Sovacool, J. Kester, *Energy Res. Soc. Sci.* **2019**, *48*, 96–107.
[3] P. G. Bruce, S. A. Freunberger, L. J. Hardwick, J.-M. Tarascon, *Nat. Mater.* **2012**, *11*, 19–29.
[4] J. Lu, K. Amine, *Energies* **2013**, *6*, 6016–6044.
[5] L. Wang, Y. Zhang, Z. Liu, L. Guo, Z. Peng, *Green Energy Environ.* **2017**, *2*, 186–203.
[6] M. M. Ottakam Thotiyl, S. A. Freunberger, Z. Peng, P. G. Bruce, *J. Am. Chem. Soc.* **2013**, *135*, 494–500.

ChemSusChem

Full Papers
doi.org/10.1002/cssc.202002317

Chemistry Europe
European Chemical
Societies Publishing

[7] J.-W. Jung, S.-H. Cho, J. S. Nam, I.-D. Kim, *Energy Storage Mater.* **2020**, *24*, 512–528.

[8] B.-W. Huang, L. Li, Y.-J. He, X.-Z. Liao, Y.-S. He, W. Zhang, Z.-F. Ma, *Electrochim. Acta* **2014**, *137*, 183–189.

[9] Y. B. Yin, J. J. Xu, Q. C. Liu, X. B. Zhang, *Adv. Mater.* **2016**, *28*, 7494–7500.

[10] R. E. Fuentes, H. R. Colón-Mercado, E. B. Fox, *J. Power Sources* **2014**, *255*, 219–222.

[11] J. Kang, O. L. Li, N. Saito, *J. Power Sources* **2014**, *261*, 156–161.

[12] Y. Jing, Z. Zhou, *ACS Catal.* **2015**, *5*, 4309–4317.

[13] H. R. Jiang, T. S. Zhao, L. Shi, P. Tan, L. An, *J. Phys. Chem. C* **2016**, *120*, 6612–6618.

[14] W.-H. Ryu, T.-H. Yoon, S. H. Song, S. Jeon, Y.-J. Park, I.-D. Kim, *Nano Lett.* **2013**, *13*, 4190–4197.

[15] W.-H. Ryu, F. S. Gittleson, M. Schwab, T. Goh, A. D. Taylor, *Nano Lett.* **2015**, *15*, 434–441.

[16] R. A. Wong, A. Dutta, C. Yang, K. Yamanaka, T. Ohta, A. Nakao, K. Waki, H. R. Byon, *Chem. Mater.* **2016**, *28*, 8006–8015.

[17] A. Nomura, K. Ito, Y. Kubo, *Sci. Rep.* **2017**, *7*, 45596.

[18] T. Liu, J. P. Vivek, E. W. Zhao, J. Lei, N. Garcia-Araez, C. P. Grey, *Chem. Rev.* **2020**, *14*, 6558–6625.

[19] D. Wang, X. Mu, P. He, H. Zhou, *Mater. Today* **2019**, *26*, 87–99.

[20] Y. Li, J. Wang, X. Li, J. Liu, D. Geng, J. Yang, R. Li, X. Sun, *Electrochem. Commun.* **2011**, *13*, 668–672.

[21] Y. Tian, H. Yue, Z. Gong, Y. Yang, *Electrochim. Acta* **2013**, *90*, 186–193.

[22] G. Xia, S. Shen, F. Zhu, J. Xie, Y. Hu, K. Zhu, J. Zhang, *Electrochem. Commun.* **2015**, *60*, 26–29.

[23] M. Salehi, Z. Shariatinia, *Electrochim. Acta* **2016**, *188*, 428–440.

[24] Y. Zhang, X. Li, M. Zhang, S. Liao, P. Dong, J. Xiao, Y. Zhang, X. Zeng, *Ceram. Int.* **2017**, *43*, 14082–14089.

[25] M. Yu, S. Zhou, Y. Liu, Z. Wang, T. Zhou, J. Zhao, Z. Zhao, J. Qiu, *Sci. China Mater.* **2017**, *60*, 415–426.

[26] Y. S. Cho, H. Kim, M. Byeon, D. Y. Kim, H. Park, Y. Jung, Y. Bae, M. Kim, D. Lee, J. Park, K. Kang, D. Im, C. R. Park, *J. Mater. Chem. A* **2020**, *8*, 4263–4273.

[27] L. M. Gilbertson, D. G. Goodwin, A. D. Taylor, L. Pfefferle, J. B. Zimmerman, *Environ. Sci. Technol.* **2014**, *48*, 5938–5945.

[28] L. M. Gilbertson, J. B. Zimmerman, D. L. Plata, J. E. Hutchison, P. T. Anastas, *Chem. Soc. Rev.* **2015**, *44*, 5758–5777.

[29] R. J. Headrick, D. E. Tsentalovich, J. Berdegué, E. A. Bengio, L. Liberman, O. Kleinerman, M. S. Lucas, Y. Talmon, M. Pasquali, *Adv. Mater.* **2018**, *30*, 1704482.

[30] G. C. Sedenho, D. De Porcellinis, Y. Jing, E. Kerr, L. M. Mejia-Mendoza, Á. Vazquez-Mayagoitia, A. Aspuru-Guzik, R. G. Gordon, F. N. Crespilho, M. J. Aziz, *ACS Appl. Mater. Interfaces* **2020**, *3*, 1933–1943.

[31] M. Park, B.-H. Kim, S. Kim, D.-S. Han, G. Kim, K.-R. Lee, *Carbon* **2011**, *49*, 811–818.

[32] N. Karousis, N. Tagmatarchis, D. Tasis, *Chem. Rev.* **2010**, *110*, 5366–5397.

[33] K. A. Wepasnick, B. A. Smith, K. E. Schrote, H. K. Wilson, S. R. Diegelmann, D. H. Fairbrother, *Carbon* **2011**, *49*, 24–36.

[34] A. Holloway, G. Wildgoose, R. Compton, L. Shao, M. H. Green, *J. Solid State Electrochem.* **2008**, *12*, 1337–1348.

[35] R. Nealer, T. P. Hendrickson, *Curr. Sustainable/Renewable Energy Rep.* **2015**, *2*, 66–73.

[36] Argonne National Laboratory, *Material and energy flows in the production of cathode and anode materials for lithium ion batteries*, Argonne, IL, **2015**.

[37] M. Zackrisson, K. Fransson, J. Hildenbrand, G. Lampic, C. O'Dwyer, *J. Cleaner Prod.* **2016**, *135*, 299–311.

[38] M. M. Falinski, D. L. Plata, S. S. Chopra, T. L. Theis, L. M. Gilbertson, J. B. Zimmerman, *Nat. Nanotechnol.* **2018**, *13*, 708–714.

[39] M. M. Falinski, M. A. Garland, S. M. Hashmi, R. L. Tanguay, J. B. Zimmerman, *Carbon* **2019**, *155*, 587–600.

[40] H. Y. Teah, T. Sato, K. Namiki, M. Asaka, K. Feng, S. Noda, *ACS Sustainable Chem. Eng.* **2020**, *8*, 1730–1740.

[41] A.-F. Trompeta, M. A. Koklioti, D. K. Perivoliotis, I. Lynch, C. A. Charitidis, *J. Cleaner Prod.* **2016**, *129*, 384–394.

[42] S. Kumar, M. Das, R. P. Singh, S. Datir, D. S. Chauhan, S. Jain, *Colloids Surf. A* **2013**, *419*, 156–165.

[43] M. N. Tchoul, W. T. Ford, G. Lolli, D. E. Resasco, S. Arepalli, *Chem. Mater.* **2007**, *19*, 5765–5772.

[44] H. Naeimi, A. Mohajeri, L. Moradi, A. M. Rashidi, *Appl. Surf. Sci.* **2009**, *256*, 631–635.

[45] G. Yamamoto, K. Shirasu, Y. Nozaka, Y. Sato, T. Takagi, T. Hashida, *Carbon* **2014**, *66*, 219–226.

[46] K. A. Wepasnick, B. A. Smith, J. L. Bitter, D. H. Fairbrother, *Anal. Bioanal. Chem.* **2010**, *396*, 1003–1014.

[47] D. C. Vennerberg, R. L. Quirino, Y. Jang, M. R. Kessler, *ACS Appl. Mater. Interfaces.* **2014**, *6*, 1835–1842.

[48] T. Chen, J. Chen, K. Waki, *Carbon* **2018**, *129*, 119–127.

[49] P. G. Collins in *Defects and disorder in carbon nanotubes*, Oxford University Press Oxford, **2009**, pp.156-184.

[50] G. S. Szymański, Z. Karpiński, S. Biniak, A. Świątkowski, *Carbon* **2002**, *40*, 2627–2639.

[51] M. Montes-Moran, D. Suarez, J. Menéndez, E. Fuente, *Carbon* **2004**, *42*, 1219–1225.

[52] N. Alexeyeva, E. Shulga, V. Kisand, I. Kink, K. Tammeveski, *J. Electroanal. Chem.* **2010**, *648*, 169–175.

[53] A. I. Belova, D. G. Kwabi, L. V. Yashina, Y. Shao-Horn, D. M. Itkis, *J. Phys. Chem. C* **2017**, *121*, 1569–1577.

[54] B. Gong, A. Ikematsu, K. Waki, *Carbon* **2017**, *114*, 526–532.

[55] K. Krumova, G. Cosa in *Overview of Reactive Oxygen Species*, *Vol. 1*, The Royal Society of Chemistry, **2016**, chap. 1, pp.1-21.

[56] F. S. Gittleson, R. E. Jones, D. K. Ward, M. E. Foster, *Energy Environ. Sci.* **2017**, *10*, 1167–1179.

[57] X. Qi, W. Song, J. Shi, *PLoS One* **2017**, *12*, e0173864.

[58] K. Rajavel, M. Lalitha, J. K. Radhakrishnan, L. Senthilkumar, R. T. Rajendra Kumar *ACS Appl. Mater. Interfaces* **2015**, *7*, 23857–23865.

[59] M. Balaish, J.-W. Jung, I.-D. Kim, Y. Ein-Eli, *Adv. Funct. Mater.* **2019**, *30*, 1808303.

[60] Q. Zhou, X. Yang, Z. Fu, C. Wang, L. Yuan, H. Zhang, Y. Tang, *Physica E* **2015**, *65*, 77–83.

[61] M. Augustin, P. E. Vullum, F. Vullum-Bruer, A. M. Svensson, *J. Power Sources* **2019**, *414*, 130–140.

[62] B. D. McCloskey, A. Speidel, R. Scheffler, D. C. Miller, V. Viswanathan, J. S. Hummelshøj, J. K. Nørskov, A. C. Luntz, *J. Phys. Chem. Lett.* **2012**, *3*, 997–1001.

[63] M. Chen, H.-W. Yu, J.-H. Chen, H.-S. Koo, *Diamond Relat. Mater.* **2007**, *16*, 1110–1115.

[64] Intergovernmental Panel on Climate Change, *Climate Change 2013 – The Physical Science Basis: Working Group I Contribution to the Fifth Assessment Report of the Intergovernmental Panel on Climate Change*, Cambridge University Press, Cambridge, **2014**

[65] M. A. Huijbregts, S. Hellweg, R. Frischknecht, H. W. Hendriks, K. Hungerbuhler, A. J. Hendriks, *Environ. Sci. Technol.* **2010**, *44*, 2189–2196.

[66] A. C. Hetherington, A. L. Borrion, O. G. Griffiths, M. C. McManus, *Int. J. Life Cycle Ass.* **2014**, *19*, 130–143.

[67] W. Zhang, Y. Shen, D. Sun, Z. Huang, Y. Huang, *Adv. Energy Mater.* **2017**, *7*, 1602938.

[68] N. Mahne, O. Fontaine, M. O. Thotiyl, M. Wilkening, S. A. Freunberger, *Chem. Sci.* **2017**, *8*, 6716–6729.